Nigerian Research Journal of Engineering and Environmental Sciences 6(2) 2021 pp. 574-586
p ISSN: 2635-3342; e ISSN: 2635-3350

Nigerian Research Journal of Engineering and Environmental Sciences
Journal homepage: www.rjees.com

Original Research Article

Identification of Welding Regime in Powder Melting

***[1]Ayoola, W.A., [2]Suder, W.J. and [2]Williams, S.W.**

[1]Department of Metallurgical and Materials Engineering, University of Lagos, Lagos State, Nigeria.
[2]Welding Engineering and Laser Processing Centre, Cranfield University, MK 43 0AL, United Kingdom.

*wayoola@unilag.edu.ng; w.j.suder@cranfield.ac.uk; s.willliams@cranfield.ac.uk

http://doi.org/10.5281/zenodo.5805165

ARTICLE INFORMATION

Article history:
Received 03 Jul, 2021
Revised 05 Nov, 2021
Accepted 26 Nov, 2021
Available online 30 Dec, 2021

Keywords:
Powder melting
Power density
Conduction welding
Weld bead profile
Beam shapes

ABSTRACT

Identification of welding regime in powder bed additive manufacturing (AM) is a complex process. This is because in solid melting with homogeneous material where heat conduction is uniform, welding regime can easily be identified. However, in powder melting, heat conduction may vary due to non-homogenous nature of the powder particles, multiple reflection and inconsistence particle-solid plate interaction. This study compared melting behaviour of solid and powder materials when the same interaction parameters and beam diameter were applied. The beam diameters investigated were from 0.10 to 6.00 mm, power density 20.4 - 5350 kW/cm^2, and interaction time between 1 - 480 ms. The results indicated that powder melting behaved differently from solid melting. For large beam diameters, layer thickness highly depends on the build height in powder melting and energy density placed significant role on depth of penetration in solid melting. The build height is higher than depth of the penetration. Thus, higher melt area was achieved in powder melting, which indicate efficient utilisation of applied energy. Comparison of solid melting to powder melting with bigger beams and the same interaction parameters showed similar conduction bead profiles. When a small beam was used, conduction bead profile achieved in powder melting spread across conduction, transition and keyhole regimes of solid melting.

1. INTRODUCTION

Laser welding, powder bed additive manufacturing (AM) and laser cladding are modern methods of fabrication. While powder bed additive manufacturing involves deposition of powder on layer-by-layer basis for the development of functional components or parts, laser cladding is often used to mitigate against surface corrosion and wear (Sampedro et al., 2011). During the AM processes, powder materials are deposited on

the surface of the substrate prior to the laser scanning. Thus, powder bed additive manufacturing and laser cladding can simply be referred to as powder melting. Laser welding is a promising technology that is used for joining and repairing different solid materials. Laser welding is very attractive for industrial applications because of the advantages such as low energy input, high localisation ability, mass production and high quality welds (Bartkowski *et al.,* 2020; Gawel 2020; Lai *et al.,* 2020).

The three regimes of solid melting in laser welding are conduction, transition and keyhole. The regimes are distinguished based on power density, interaction time and weld bead characteristic i.e., shape and quality (Assuncao *et al.,* 2010; Ayoola *et al.,* 2017). Conduction welding requires a low power density to avoid material vaporisation. Depending on the beam diameter, the process usually involves longer interaction times than keyhole to enable the heat to conduct inside of the material (Ayoola *et al.,* 2019). The seam has a relatively shallow depth of penetration and good surface finish with on spatial generation. In the keyhole regime, the incident power density delivered to the workpiece surface is high enough to initiate local vaporisation of the metal. As the power density is increased further, the cavity becomes deeper and a keyhole is formed (Suder and Williams 2012). The keyhole formed in the molten metal enable deep penetration of laser beam into the material, resulting in a weld profile poor surface finishing. The ratio of the depth of penetration to the weld width (the aspect ratio) is another basic factor that helps distinguish conduction welds from keyhole welds. In conduction and keyhole regimes, the aspect ratio increases significantly with increasing power density and energy density. The transition regime shows a gradual increment of aspect ratio with increasing power density and energy density. According to Assuncao *et al.* (2012), the maximum aspect ratio for conduction regime is 0.40, for transition regime is between 0.40 and 0.60 while welds with aspect ratio above 0.60 are in keyhole regime. Thus, both applied power density and the aspect ratio is important for the regime identification. The main advantages of classifying welding regimes are to understand the process and its uses (Morgan and Williams, 2002).

Identification of powder bed additive manufacturing regime may be complex. This is because metal vaporisation and build defects are not desirable. Therefore, the applied power density and energy need to be precisely controlled to know the welding regime. To control the amount of applied energy, the laser power and travel speed are often varied depending on the beam diameter, powder particle sizes and layer thickness required to fuse each path. In this way, the melting process is either in conduction regime or keyhole regime. In laser conduction welding, the aspect ratio is less than or equal to 0.5. Thus, weld bead profile can be classified as a disc or point source (Sánchez-Amaya *et al.,* 2009; Assuncao *et al.,* 2012; Chelladurai *et al.,* 2014). The mechanism of heat propagation within the material is by heat conduction (King *et al.,* 2014). Similarly, in powder bed AM, to achieve intimate wetting between a liquid metal and solid substrate underlying, there is a maximum ratio of track length to width (diameter) that can prevent capillary instability (Song *et al.,* 2014). The deposited build profile has to be semi-circle. Considering this relationship, each layer in powder bed system may be treated as conduction weld. In reality to achieve high resolution, it is a common practice to reduce the beam diameter. Therefore, the smaller the spot size becomes, the higher the power density required for the melting. For material of similar properties, the power density and interaction time change with the beam diameter. Thus, the powder bed regime may be changing with beam diameter. A keyhole mode laser melting was observed in a laser powder-bed fusion process (King *et al.,* 2014).

The objective of this study is to compare the solid and powder melting when the same interaction parameters and beam diameters are used. The bead profile of solid melting will be compared with the build height of powder melting and the interaction parameters that control the process will be examined.

2. MATERIALS AND METHODS

2.1. Laser Sources

Two sources of laser power were used. The first was high power IPGYLR-8000 continuous wave (CW) fibre laser with an output of 8000 W. This source of laser was used for the solid and powder melting in case of large beam diameters. The second source was medium power fibre laser with maximum output of 500 W for

the smaller beam diameters. The high-power laser was used in out of focus position to achieve wider beam diameters and the medium fibre laser was focused. The details of the properties of the two lasers are shown in Table 1.

Table 1: Beam properties of the two sources of laser used for this study

Beam properties	IPGYLR -8000	JK500FL
Laser power (W)	8000	500
Wavelength (µm)	1.07	1.07
Optical fibre diameter (mm)	300	300
Collimating lens	125	115
Focusing lens length (mm)	250	300
Beam diameter (mm)	4.0 and 5.0	0.10

2.2. Processing Chamber for Large Beam Diameters

A processing chamber was used for powder and solid melting with both high and medium power lasers. The set-up consisted of the laser system, the constructed chamber, system control unit and the simple motion mechanism. The laser emission was delivered to the workpiece through an optical window allocated in the top surface of the chamber, as shown in Figure 1. Thus, the laser energy was delivered through the optical window. To prevent laser head from back reflection, the optical head was tilted at an angle of 10^{o}. In initial experiments conducted in solid and powder melting, the effect of shielding gas was not significant on the bead profile. Therefore, with large beam diameters, no shielding gas was used for solid and powder melting.

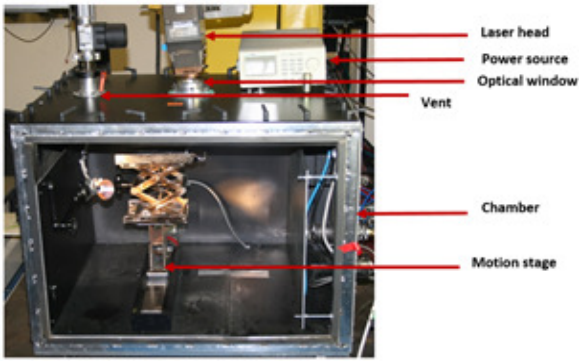

Figure 1: Experimental set-up used for the small and large beam diameters

2.3. Processing Chamber for Small Beam Diameter

The sample set-up shown in Figure 1 was used for solid and powder melting with small beam diameters. The basic difference in the chamber was that it was airtight with argon gas for the case of small beam diameter. Argon gas was supplied through the air knife to provide oxygen free environment and to protect the optical window from contamination. The shielding gas was used for the process because of the small conduction welds been produced and some welds are also in keyhole regime. The oxygen level maintained was less than 500 ppm. Low power laser from SPI was used for this experiment.

2.4. Sample Preparation and Welding Parameters

S275 mild steel was used as the substrate material for the powder and solid melting. For powder melting, two groove depths of 0.50 and 1.00 mm were used for the large beams (4.00 mm and 5.00 mm) and 0.20 mm for small beam (0.1 mm), as in Figure 2. The width and length of each of the grooves was 10 mm x 90 mm respectively. The groove depths served as the layer thickness for the powder melting. Prior to powder and solid melting, all the plates with and without grooves were thoroughly cleaned with acetone solution. For solid melting, the samples were coated with graphite spray. This is to minimise variations of the absorptivity of the laser radiation. The cleaned grooves were allowed to dry and then filled with iron powder

for the powder melting. The average particle size of the powder was ≤ 0.15 mm and used in as-received condition. The powder materials used was nitrogen atomised pure iron supplied by Sandvik Osprey Ltd. This powder was selected due to its close composition to the solid steel used in this work. The powder materials were treated with minimum exposure to the atmosphere to reduce the absorption of moisture and prevent its contamination.

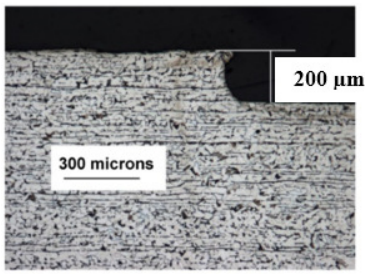

Figure 2: A groove of 0.20 mm used for powder melting with a bead diameter of 0.10 mm

The welding parameters were adjusted to the beam diameters according to Equations 1 and 2 to obtain power density and interaction time respectively. Other power densities used for the large beams were 20.4 kW/cm^2, 22.9 kW/cm^2 and 25.5 kW/cm^2 and small beam were 1150 kW/cm^2, 1660 kW/cm^2, 2160 kW/cm^2, 2670 kW/cm^2, 3570 kW/cm^2 and 5350 kW/cm^2. The product of the interaction time and power density is defined as the energy density, as in Equation 3. The interaction parameters used to compare the melting behaviour of solid and powder materials for large and small beam diameters are shown in Tables 2 and 3 respectively. Throughout experiments, high speed imaging was used to observe the melting behaviour of both powder and solid melting.

$$Power\ density\ (P_d) = \frac{Laser\ power}{Area\ of\ the\ laser\ spot} \quad (1)$$

$$Interaction\ time\ (t_i) = \frac{Laser\ spot\ diameter}{Laser\ travel\ speed} \quad (2)$$

$$Energy\ density\ (E_d) = P_d * t_i \quad (3)$$

Table 2: Parameters used to compare solid and powder melting with beam diameter of 4.0 mm and 5.0 mm and power density of 28 kW/cm^2

BD (mm)	4	5	6
$\boldsymbol{t_i}$ $(\boldsymbol{ms})$	t_s (mms^{-1})	t_s (mms^{-1})	E_d (kJ/cm^2)
60	66.00	83.30	1.70
120	33.20	41.70	3.40
240	16.67	20.80	6.70
480	8.33	10.40	13.50

Table 3: Parameters used to compare solid and powder melting with beam diameter 0.10 mm and power density of 640 kW/cm^2

$\boldsymbol{t_i}$ $(\boldsymbol{ms})$	$\boldsymbol{t_s}$ $(\boldsymbol{mms^{-1}})$	$\boldsymbol{E_d}$(kJ/cm^2)
1	100.0	0.60
2	50.0	1.30
4	25.0	2.50
6	16.7	3.80
8	12.5	5.10
10	10.0	6.40

3. RESULTS AND DISCUSSION

This study compared the melting behaviour of homogeneous solid material and non-homogeneous of powder particles distribution. Table 4 shows the bead-on-plate welds of solid material and fused tracks of powder at the same energy density (product of interaction time and powder density) and beam diameter. In solid material, bead-on-plate weld was achieved for all energy densities investigated. In contrast, fusion of the powder on the substrate was achieved only with groove depth of 0.5 mm for all energy densities. No fusion was achieved when the groove depth was increased from 0.5 mm to 1.0 mm at energy density of 17 J/mm^2 and beam diameter 4.0 mm. Similarly, partial fusion can be seen for bead diameter of 5.0 mm. This implies that certain amount of energy density is required to achieve complete fusion of powder on the substrate. The required energy density varies with the groove depth (layer thickness) and the beam diameter. For instance, when the groove depth was increased at constant beam diameter and energy density, there was a lack of fusion due to increase in powder volume. However, when the beam diameter was increased at constant layer thickness and energy density, complete or partial fusion was achieved. This is because there is an increase in the specific point energy when the applied energy density is constant (Suder and Williams 2012). This significantly enhanced the fusion process. Specific point energy (Equation 4) defines the area over which certain amount of energy density is applied. Olakanmi (2013) also defined energy density as the ratio of laser power to the travel speed, layer thickness and scan spacing (J/mm^3). The equation combined significant effect of layer thickness and scan spacing. The equation was adapted to powder melting process with multiple layers.

$$E_s = E_d * A_d \tag{4}$$

Table 4: Bead-on-plate welds of solid melting and build layers of powder melting produced with the same interaction parameters and beam diameters (d_b)

P_d = 28 kW/cm^2	t_i (ms)	Powder melting: Groove depth = 0.5 mm and (d_b) = 4 mm	Powder melting: Groove depth = 0.5 mm and (d_b) = 5 mm	Powder melting: Groove depth = 1.0 mm and (d_b) = 4 mm	Powder melting: Groove depth = 1.0 mm and (d_b) = 5 mm	Solid melting: Weld profile of (d_b) = 4mm	Solid melting: Weld profile of (d_b) = 5 mm
$E_d = 17J/mm^2$	60	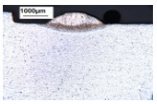	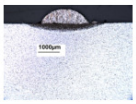	No fusion	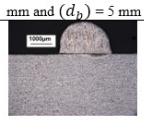 (Partial fused)	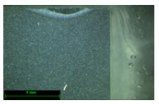	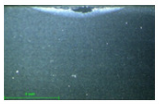
$E_d = 34J/mm^2$	120	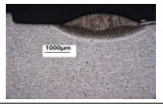	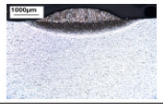	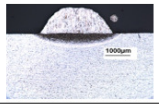		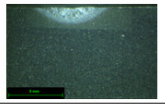	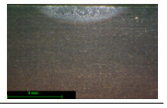
$E_d = 67J/mm^2$	240			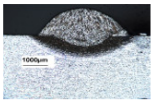	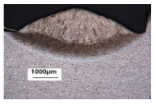	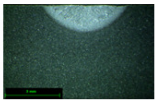	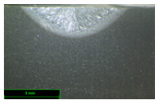
$E_d = 135J/mm^2$	480		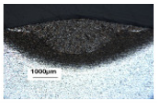	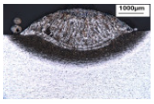		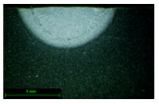	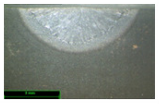

Figure 3 shows the depth of penetration and build height as a function of the energy density. It can be seen that for the same energy density, the build height is slightly higher than depth of penetration, with some significant fusion zone in the substrate of powder melting. Figure 4 also confirmed such a trend. In solid melting, the interaction parameters that mainly control the depth of penetration is interaction time and the weld width are the interaction time and beam diameter (Ayoola et al., 2017). Depth of penetration increases with increasing interaction time as shown in Table 4 and Figure 3. In powder melting, the melting behaviour is different from that of solid melting in some ways. The main parameter that control the build height in powder melting is the layer thickness. As expected, when the layer thickness doubled, the build height also increased by a factor of two for the same energy applied, when the energy was sufficient. Increasing of the energy density from 17 J/mm^2 to 135 J/mm^2 caused no significant difference in build height, as shown in

Table 3 and Figure 4. When the thickness of powder layer is greater than the energy required to fuse it completely to the substrate, the molten pool solidifies rapidly and there is not enough time for bonding with the substrate. Then build height formed is higher than layer thickness because the surface tension pulls the liquid pool (see Figure 5). The surface tension which is a function of temperature. The low temperature of liquid results in strong surface tension, which forces the liquid metal to reduce its surface energy by attaining circular shape (Tolochko *et al.,* 2004; Gusarov *et al.*, 2007). Poor wetting and strong surface tension due to the low temperature of the liquid is responsible for the lack of fusion between the powder particles and the substrate. This behaviour depends on the powder size and layer thickness. Lack of fusion occurs when the energy absorbed is not sufficient for wetting between the powder particles and the substrate. At a higher energy density, the dilution between melted powder and the substrate will increase with less effect on the build height. This behaviour is shown in Table 3 and Figure 4. The percent reduction in build height for layer thicknesses of 0.5 and 1.0 mm was 10 % (maximum) when the energy density was increased from 17 J/mm^2 to 135 J/mm^2.

Figure 6 shows the comparison of weld and build widths for the same energy density and beam diameter. The weld width is slightly higher than the build width at lower energy density for both beam diameters. However, at higher energy density, there is no significant difference in the weld and build width. Figure 7 also confirmed the trend for a wider range of parameters. Interaction time and beam diameter control the weld width profile in conduction welding (see Figures 6 and 7) for solid melting with large beams (Ayoola *et al.,* 2017). The same parameters control the build width in powder melting. Both the weld and build widths reach saturation at the point where they approach the size of the beam on the workpiece. Greater energy, which is required to achieve melting with larger beam diameters, leads to a bigger melt pool and longer solidification time. In that case, the melt flow has a significant influence on width bead profile. Therefore, when the applied energy density is sufficient to fuse a given layer thickness, the build height is not sensitive to the beam diameter but build widths.

Tables 5 and 6 show the process maps of the bead-on-plate welds (solid melting) and built layers (powder melting) produced with a beam diameter of 0.10 mm and interaction parameters shown in Table 2. The welds exhibit conduction profiles when the power density applied was equal to or less than 2.67 MW/cm^2 with interaction time less than 8 ms as presented in Table 5. The depth of penetration is shallow and weld width is wide at lower power density, as shown in Figure 8a and Figure 9a. There was a significant increase in the aspect ratio (depth/width) of the welds beyond power density of 2.67 MW/cm^2 and interaction time of 8 ms leading to welds of transition or keyhole characteristics. For instance, the weld produced with power density of 5350 kW/cm^2 show characteristics of keyhole regime with an aspect ratio greater than 0.6 (Figures 10 and 11). There are four main regions of the build layers process map (Table 6). The first region is where there is no melting but heating of the powder. In the second region, there is a melting of the powder layer, however, due to insufficient heating the wetting of the molten powder with the substrate is inadequate and the deposited bead attains a ball shape. In the third region, there is a significant melting of the powder layer deposited. The built layers produced form a circular cross section with little wetting between the built layer and the substrate. The portion of the build width fused into the substrate is smaller than the diameter of the deposits. The fourth region is where there a complete melting of powder and smooth deposits.

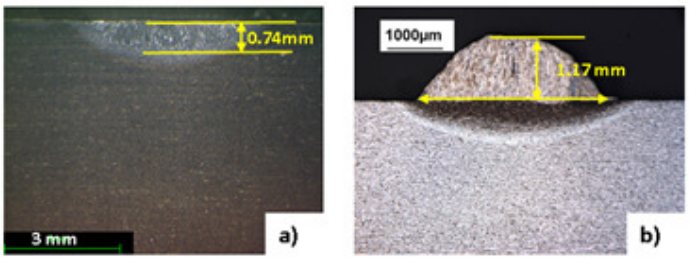

Figure 3: Comparison of the depth of penetration with build height at a constant energy density of 34 J/mm^2 (28 kW/cm^2 and 120 ms) and beam diameter of 5.00 mm for a) solid melting and b) powder melting

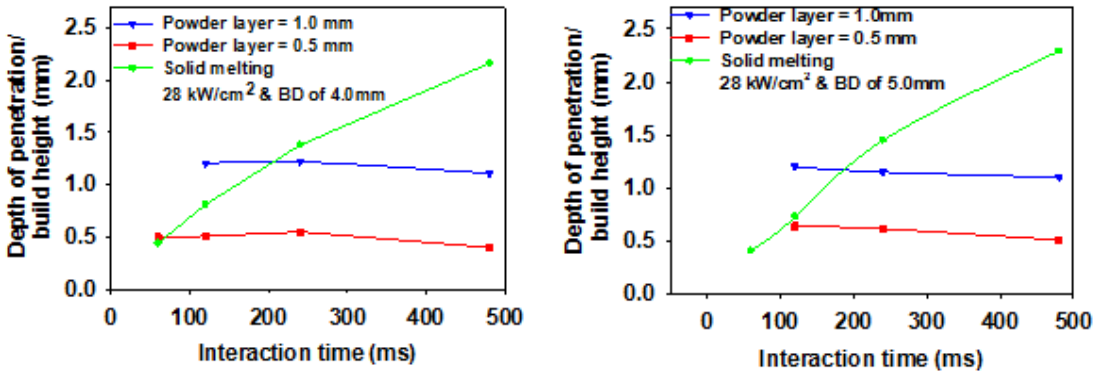

(a) (b)

Figure 4: Comparison of the depth of penetration with build height for the same energy density and layer thickness for beam diameters of (a) 4.0 mm and (b) 5.0 mm (Note: green lines are penetration in solid melting)

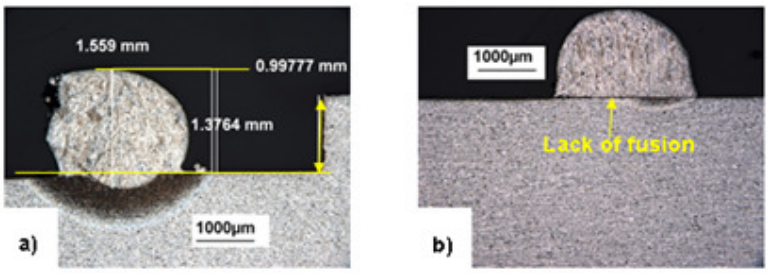

Figure 5: Examples of defects in powder melting a) humping formation b) lack of fusion below minimum energy for fusion

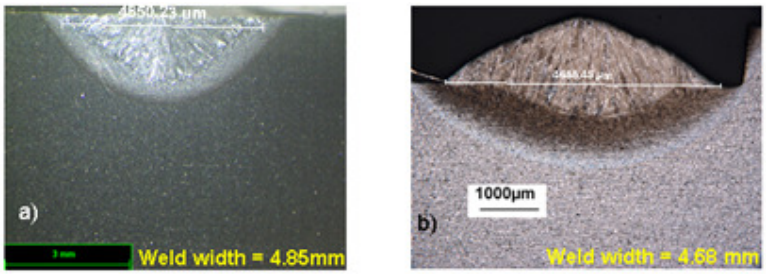

Figure 6: Comparison of weld width with build width produced with energy density of 6.7 kJ/cm^2 (28 kW/cm^2 and 240 ms) and beam diameter of 5.00 mm a) solid melting and b) powder melting

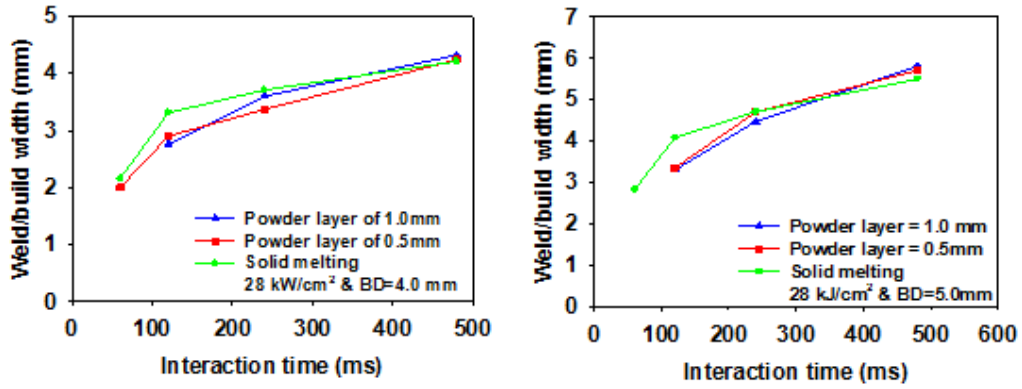

(a) (b)

Figure 7: Comparison of the weld width with build width for the same energy density and layer thickness for beam diameters of (a) 4.0 mm and (b) 5.0 mm (Note: green lines are penetration in solid melting)

Table 5: Process map of the bead-on-plate-welds (solid melting) produced with different combinations of interaction parameters. Key C: conduction weld, T: transition welds and K: keyhole welds

Power density (kW/cm²)	Interaction time (ms)					
	1	2	4	6	8	10
640	C	C	C	C	C	C
1150	C	C	C	C	C	C
1660	C	C	C	C	C	C
2160	C	C	C	C	C	C
2670	C	C	C	C	C	C
3570	C	C	T	T	T	K
5350	K	K	K	K	K	K

Table 6: Built layer of powder melting produced with different combinations of interaction parameters. Key - N: No melting, B: balling formation, x: balling and discontinuity and +: smooth bead and melting

Power density (kW/cm²)	Interaction time (ms)					
	1	2	4	6	8	10
640	N	B	B	B	B	B
1150	x	x	x	x	x	x
1660	x	x	x	x	x	+
2160	x	x	x	+	+	+
2670	+	+	+	+	+	+
3570	+	+	+	+	+	+
5350	+	+	+	+	+	+

Figure 8 to Figure 10 show comparison of selected bead-on-plate welds and powder-built layers. Some build layers in powder exhibit lack of fusion between the layers and the substrate. The powder layer thickness in every case was much greater than the penetration depth in conduction welding of the solid material (Figure 8a). It can also be seen in the single layer deposited tracks that the profile exhibits lack of continuity and balling due to insufficient energy for this thickness of powder layer (Figure 8b). The macrographs of the build layers with complete fusion are presented in Figure 9, Figure 10a, and Figure 11a. The corresponding single track of layers are presented in Figure 10b and Figure 11b. These figures indicate that the build layers are relatively smooth and stable, because of greater energy input. Furthermore, the build height of powder melting is significantly higher than the depth of penetration of conduction welding of solid melting. The comparison of the build width and weld width, on the other hand indicates that the profiles are equal only when the process is in steady state. Thus, the melt volume of the powder is higher than the melt area of the substrate, which indicates better utilisation of laser energy in powder melting than in conduction welding. Figure 11 shows bead of keyhole profile for solid melting and conduction profile for powder melting. This indicates that build profile formed is largely dependent on the interaction parameters and powder properties.

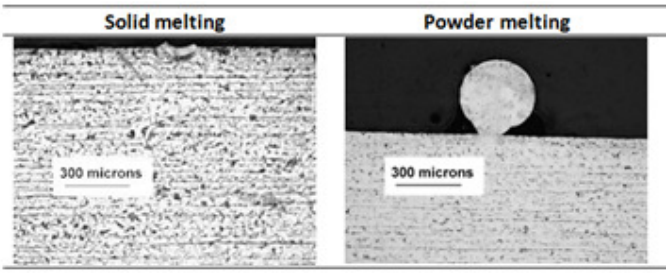

Figure 8a: Comparison of bead-on-plate weld with a single layer powder deposition at constant power density of 640 kW/cm^2, interaction time of 10 ms and layer thickness of 0.2 mm

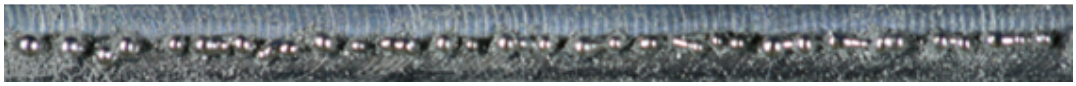

Figure 8b: Top view of deposited track for 0.2 mm powder layer thickness, power density of 640 kW/cm^2 and interaction time of 10 ms

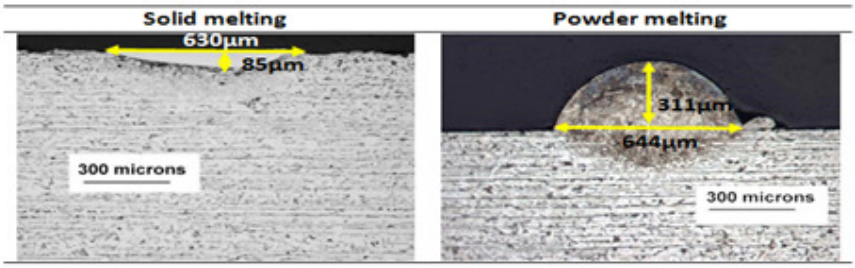

Figure 9: Comparison of bead on plate weld with a single layer powder deposition at constant power density of 2670 kW/cm^2, interaction time of 4 ms and layer thickness of 0.2 mm

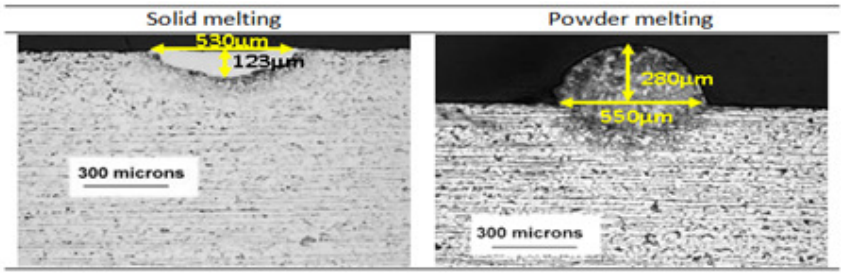

Figure 10a: Comparison of bead on plate weld with a single layer powder deposition at constant power density of 2670 kW/cm^2, interaction time of 8 ms and layer thickness of 0.2 mm

Figure 10b: Top view of deposited tracks for 0.2 mm powder layer thickness, power density of 2670 kW/cm^2 and interaction time of 8 ms

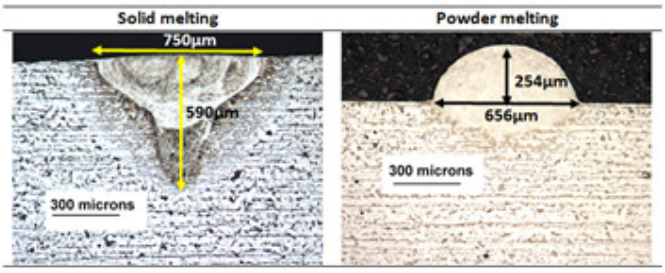

Figure 11a: Comparison of bead on plate weld with a single layer powder deposition at constant power density of 5350 kW/cm^2, interaction time of 2 ms and layer thickness of 0.2 mm

Figure 11b: Top view of deposited tracks for 0.2 mm powder layer thickness, power density of 5350 kW/cm^2 and interaction time of 2 ms

Powder melting is more efficient than solid melting when the same interaction parameters are applied. In large beam diameters, the build height is slightly higher than the depth of penetration while the weld and build widths are similar. This implies that melt area in powder is higher than weld area. The melt behaviour with small beams was different from that of large beams. The build height in powder was significantly higher than the depth of penetration in solids. The weld and build widths were significantly wider than the beam diameter for both solids and powders. The result is that powder exhibited higher melt area than solid material. This shows that in these regimes powder melting is more efficient than solid melting. The difference in melt area between solid material and powder material becomes more significant for smaller beam diameters. Within the region of conduction weld profiles in solid melting, powder melting is more efficient. However, in keyhole or transition regime, solid melting exhibited a similar or higher melt area (see Figure 11).

The higher build area obtained in powder melting compared to the weld area in solid melting is likely to be due to the difference in the energy utilised for melting (i.e. as opposed to that lost due to reflection from the surface and that is lost to heating the surrounding material). Both powder and solid substrate absorbed energy whilst exposed to the laser beam. However, the extent of the energy utilised for melting depends on the material properties thermal diffusivity, surface roughness, oxidation state. In powder melting, due to the higher surface roughness of the powder, there are multiple reflections, which enhance the laser absorption in the powder. In addition, powder materials are characterised with lower thermal diffusivity because of the presences of voids. The large spaces between the powder particles lead to a very low effective thermal conductivity. This means that the lateral thermal losses would be much lower leading to higher energy utilisation and therefore melt area. Furthermore, it is expected that there might be significant shrinkage of the build profile due to the voids between the particles and their random arrangement. The build height results obtained indicate that the build height is higher or the same as the layer thickness for build layer of proper deposition when applied energy is sufficient. However, molten metal shrinkage does not seem to affect the build profile. The fact is that the low conduction losses in powder melting are compensated for the low thermal diffusivity.

Within the interaction parameters investigated for the small beam, three regimes of conduction, transition and keyhole were observed in solid melting. In the first regime, the welds exhibited less or semi-circle profile and the second region consisted of welds of transition and keyhole profiles of deeper penetration, as shown in Table 6. Powder melting consisted of four regions. In the first region no melting but heating of the powder by the laser energy occurs. In this region, there are no physical changes or bonding between the adjacent powder particles. In the second region, there is a significant melting. The agglomerated powder particles spheroidise because of high surface tension. The size and shape formed depend on the applied energy density.

The third region consists of significant melting and clustering of the powder particles. Smooth build achieved in the fourth region. Full melting of powder particles occurred due to the interaction between the laser beam and powder. In this case, the melt pool was similar to conduction welding in solid material, which formed stable beads with little dilution. The balling effect was completely absent in this region. This implies that a certain threshold energy density is required to melt and fuse a particular layer of powder. The energy has to overcome losses into the substrate (melting into the substrate beneath) and melting of the powder. Therefore, the solidification time needs to be long enough to provide good wetting between powder particles and the substrate. By comparing the bead profiles of solid melting to the powder melting, the region with no melting and balling corresponded to the conduction welding regime in solid melting. This implies that the applied interaction time and power density is too low for build layer formation but sufficient for surface melting. The powder layer serves as screening surface. Thus, little energy could reach the substrate and no bonding in this low energy regime occurs. On further increase of the energy density (power density or interaction time), the surface free energy decreases (lower surface tension) causing the powder particle to agglomerate into the melt pool and resulting in further transfer of heat and melting. The semi-circular build profile achieved in powder melting corresponded to conduction, transition and keyhole regimes in solid melting. This implies that interaction parameters for conduction, transition or keyhole welding in solids all correspond to stable build layers.

Similar to solids, three welding regimes are possible in powder melting, conduction, transition and keyhole. All the build layers shown with the large beam diameters are in conduction mode (Table 4). Those with longer transition times or higher energy densities (67 J/mm^2 or 135 J/mm^2) show significant penetration into the substrate but would still be considered as conduction welds. For the small (0.10 mm) beam diameter, profiles shown in Figures 9 and 10 for the builds that are fully fused to the substrate, the profiles are mainly those of conduction regime. The particle size was similar to that of the layer height with laser beam diameter being smaller. It seems likely that the keyhole profiles maybe formed when the laser beam passed through a gap between the powder particles and interacted directly with the substrate, as shown in Figure 12.

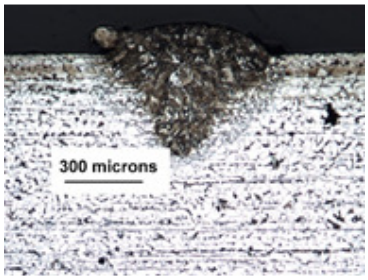

Figure 12: Deposited tracks for 0.2 mm powder layer thickness, power density of 5350 kW/cm^2 and interaction time of 2 ms with keyhole characteristic

It is clear from the comparison between solid and powder melting that although when solid melting is in transition or keyhole mode, powder melting is still in conduction mode. A clear example of this is shown in Figure 10a and Figure 11a. This means that the welding regime in powders is different to that of solid materials under the same conditions when the laser beam diameter is of the order of the powder particle size. Given that, this is the case in most powder bed systems this is a very important observation. Camera observation of the powder melting with large diameter shown in Figure 13 gives the impression that the process is operating in the keyhole welding regime with evidence of high spatter levels while the solid melting counterpart shown no spatter. It is clear that if a solid material is put directly in a powder bed system (with small beams) then conduction, transition and keyhole welds are the results in solid material while conduction result in powder melting. This means that it may be difficult to form a keyhole in powder materials in the same way as in solid, especially when the beam size is comparable to that of the powder particles. The spatter that is observed in powder bed systems may be the result of individual particles being ejected due to local vapourisation.

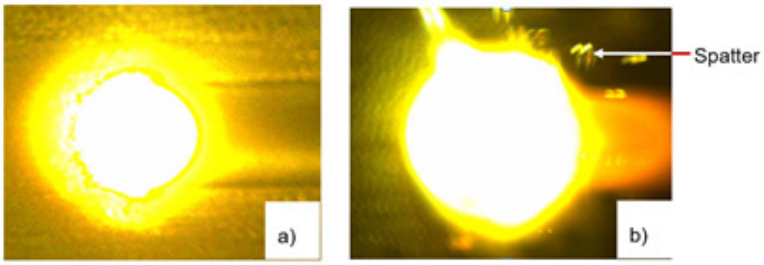

Figure 13: Melting characteristics in two different materials for the same processing conditions (a) solid melting (b) powder melting

4. CONCLUSION

The following conclusions can be drawn from this study

i. A profile of the bead formed during melting of solid or powder depends on the beam diameter and welding regimes.
ii. The parameters that control build heights in powder melting are the thickness of powder layer and energy density (power density and interaction time).
iii. Greater melting area was found in powder as compared to solid, especially for small beam diameters. In addition, powder melting exhibited more spatter and expulsion than solid material, for the same processing parameters.
iv. The welding regime of powder melting was investigated by comparing the weld profile in solids to the build profile in powders when the same interaction parameters are applied. It has been found that most of the build profiles indicated conduction welding only.

5. ACKNOWLEDGMENT

This research effort was funded by EPSRC Centre for Innovative Manufacturing in Laser based Production grant number EP/ J017086/1. The authors are also grateful to Petroleum Technology Development Fund (PTDF) Nigeria for the student support.

6. CONFLICT OF INTEREST

There is no conflict of interest associated with this work.

REFERENCES

Assuncao, E., Ganguly, S., Yapp D. and Williams, S. (2010). Conduction mode broadening the range of applications for laser welding, In: *63th Annual Assembly and International Conference of the International Institute of Welding*, pp. 705–709.

Assuncao, E., Williams, S. and Yapp, D. (2012). Interaction time and beam diameter effects on the conduction mode limit. *Optics and Lasers in Engineering,* 50, pp. 823–828.

Ayoola, W. A., Suder W. J. and Williams S. W. (2019). Effect of beam shape and spatial energy distribution on weld bead geometry in conduction welding. *Optical and laser Technology,* 117, pp. 280 – 287.

Ayoola, W. A., Suder, W. J. and Williams, W. S. (2017). Parameters controlling weld bead profile in conduction welding. *Journal of Materials Technology,* 249, pp. 522-530.

Bartkowski, D., Bartkowska, A., Piasecki, A. and Jurci, P. (2020). Influence of laser cladding parameters on microstructure, microhardness, chemical composition, wear and corrosion resistance of Fe-B composite coating reinforced with B4C and Si particles. *Coatings,* 10, (809), pp. 1-18.

Chelladurai, A. M., Gopal, K. A., Murugan, S., Venugopal, S. and Jayakumar, T. (2012). Energy transfer modes in pulsed laser seam welding. *Materials and Manufacturing Process,* 30**,** pp. 162–168.

Gawel, T. G. (2020). Review of Additive manufacturing. *Solid State Phenomena*, 308, pp. 1-20.

Gusarov, A. V., Yadroitsev, I., Bertrand, P. and Smurov, I. (2007). Heat transfer modelling and stability analysis of selective laser melting. *Applied Surface Science.* 254, pp. 975–979.

King, W. E., Barth, H. D., Kamath C., Gallegos, G. F. and Gibbs, J. W. (2014). Observation of keyhole-mode laser melting in laser powder-bed fusion additive manufacturing. *Journal of Materials Processing Technology,* 214, pp. 2915–2925.

Lai, W. J., Ganguly, S. and Suder, W. (2020). Study on effect of laser keyhole weld termination regimes and material composition on weld overlap defects, *Journal of Manufacturing Processes,* 58, pp. 416-428.

Morgan, S. A. and Williams, S. W. (2002). Hybrid laser conduction welding. 55th Annual *Assemebly of Interactional Institute of Welding*.

Olakanmi, E. O. (2013). Selective laser sintering/melting (SLS/SLM) of pure Al, Al-Mg, and Al-Si powders: Effect of processing conditions and powder properties. *Journal of Materials Processing Technology*, 213, pp. 1387–1405.

Sampedro, J., Perez, I., Carcel, B., Ramos, J. A. and Amigo, V. (2011). Laser cladding of TiC for titanium components. Physics Procedia, 12, pp. 313-323.

Sánchez-Amaya, J. M., Delgado, T., González-Rovira, L. and Botana, F. J., (2009). Laser welding of aluminium alloys 5083 and 6082 under conduction regime. *Applied Surface Science*, 255, pp. 9512–9521.

Song, B., Dong, S., Zhang, B., Kiao, H. and Coddet, C. (2014). Effects of processing parameters on microstructure and mechanical property of selective laser melted Ti6Al4V, *Materials and Design. 35*, pp. 120 – 125.

Suder, W. J. and Williams, S. W. (2012). Investigation of the effects of basic laser material interaction parameters in laser welding. *Journal of laser application,* 24(3), pp. 032009.

Tolochko, N. K., Mozzharov, S. E., Yadroitsev, I. A., Laoui, T., Froyen, L., Titov, V. and Ignatiev, M. B. (2004). Balling processes during selective laser treatment of powders. *Rapid Prototyping Journal,* 10, pp. 78 – 87.